

# Metal-to-insulator transition and electron-hole puddle formation in disordered graphene nanoribbons

Gerald Schubert and Holger Fehske

*Institut für Physik, Ernst-Moritz-Arndt-Universität Greifswald, 17487 Greifswald, Germany*

(Dated: June 7, 2021)

The experimentally observed metal-to-insulator transition in hydrogenated graphene is numerically confirmed for actual sized graphene samples and realistic impurity concentrations. The eigenstates of our tight-binding model with substitutional disorder corroborate the formation of electron-hole- puddles with characteristic length scales comparable to the ones found in experiments. The puddles cause charge inhomogeneities and tend to suppress Anderson localization. Even though, monitoring the charge carrier quantum dynamics and performing a finite-size scaling of the local density of states distribution, we find strong evidence for the existence of localized states in graphene nanoribbons with short-range but also correlated long-range disorder.

PACS numbers: 71.23.An,72.15.Rn,71.30.+h,05.60.Gg

The experimental observation of a disorder-induced metal-to-insulator transition in graphene upon hydrogenation [1] has triggered a vivid debate on the nature of this transition. For high concentrations of hydrogen several mechanisms of gap opening have been discussed, such as full  $sp^2$  to  $sp^3$  transition, localization of  $sp^3$  areas, or erasing of midgap states [2] [3]. Graphene, on the other hand, is a truly two-dimensional system, and the one-parameter scaling theory predicts that at zero temperature any finite amount of disorder should lead to Anderson localization (AL) [4]. Otherwise, the existence of a scaling function might be questionable since the Fermi wavelength diverges near the charge neutrality point and there is no spatial scale on which the conductivity is much larger than  $e^2/h$  [5]. So far it seems that AL has not been seen in disordered graphene down to temperatures of liquid-helium [6]. This surprising result has been attributed to strong charge carrier density fluctuations that break up the sample into electron-hole puddles [7]. Within these puddles the local chemical potential deviates enough from the charge neutrality point to allow for electron or hole conductivity. Mesoscopic transport is then determined by activated (variable-range) hopping or leakage between the puddles [8]. If the formation of electron-hole puddles is suppressed, however, AL might be observed. This has been reported by quite recent experiments in double-layer graphene heterostructures [9].

Previous theoretical work on disordered graphene strongly emphasizes the difference between short- and long-range scatterers. While the former applies to the case of hydrogenation, the latter rather describes the effect of charged impurities in the substrate [10]. Within the Dirac approximation, only short-range impurities cause intervalley scattering, and thus may lead to AL [11]. The presence of long-range impurities alone gives rise to intravalley scattering which is not sufficient to localize the charge carriers [12]. Another factor is the edge geometry of the graphene nanoribbons (GNRs) that determines the universality class of disordered samples

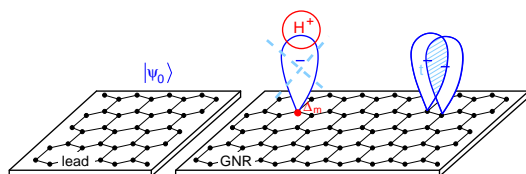


FIG. 1. (Color online) Cartoon of the substitutional disorder model describing hydrogenated graphene.

as long as the phase coherence length exceeds the system size [13]. Going beyond the Dirac approximation and describing graphene by a tight-binding model, it is natural to ask whether the scattering range is still decisive. Deviations from the idealized linear dispersion, a finite lattice spacing, and the trigonal lattice symmetry, which breaks the rotational symmetry of the Dirac cones, call for a careful numerical analysis of the localization properties within the tight-binding description [14].

In this work, we prove by unbiased numerics that experimentally relevant concentrations of hydrogen  $x \ll 1$  may induce a metal-to-insulator transition in actual-size graphene samples. We show that the single-particle wavefunctions of our disorder model are also localized for correlated long-range disorder. Even for potential fluctuations on an atomistic scale there is strong evidence for electron-hole puddle formation on an intrinsic scale of some ten nm, in agreement with recent experimental observations. [15]. In contrast to previous studies on temperature dependent transport in disordered graphene within the semiclassical Boltzmann approach [16], we restrict ourselves in the following to strictly zero temperature and adopt a purely quantum point of view.

We consider a tight-binding Hamiltonian  $H = -t \sum_{\langle ij \rangle} (c_i^\dagger c_j + \text{H.c.}) + \sum_i V_i c_i^\dagger c_i$ , on the honeycomb lattice with  $N$  sites, where the operators  $c_i^\dagger$  ( $c_i$ ) create (annihilate) an electron in a Wannier state centered at site  $i$ , and  $t$  denotes the nearest-neighbor transfer integral. The landscape of onsite potentials  $\{V_i\}$  results

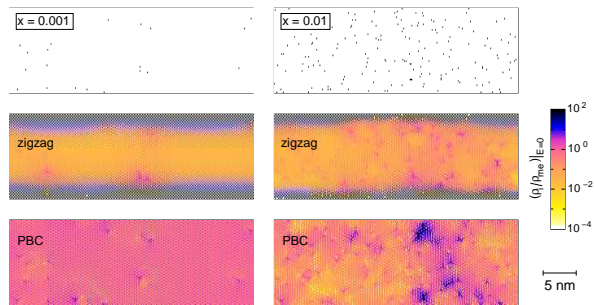


FIG. 2. (Color online) Spatial distribution of the normalized LDOS  $\rho_i/\rho_{me}$  at  $E = 0$  for the binary alloy model with potential difference  $\Delta = 6.0t$  and impurity concentration  $x = 0.1\%$  (left column) and  $1\%$  (right column). The disorder configurations shown in the top panel were used for both BC. Data obtained by exact diagonalization (ED), GNR sample size  $(37 \times 12) \text{ nm}^2$ , corresponding to  $300 \times 60$  atoms.

from the superposition of contributions of  $N_{\text{imp}} = xN$  randomly distributed Gaussian impurities at positions  $\mathbf{r}_m$  [17]:  $V_i = \sum_{m=1}^{N_{\text{imp}}} \Delta_m \exp(-|\mathbf{r}_i - \mathbf{r}_m|^2/(2\xi^2))$ . By choice of  $\xi$  the range of the individual impurity potentials can be continuously tuned from short-ranged to long-ranged. For  $\xi \rightarrow 0$  and  $x = 1$  we recover the Anderson model on a GNR [18]. Assuming a fixed  $\Delta_m = \Delta$  for all impurities, the limit  $\xi \rightarrow 0$  results in the binary alloy model in which only distinct sites acquire a finite onsite potential. Vacancies correspond to sites with  $\Delta \rightarrow \infty$ , leading to a quantum site-percolation scenario [19]. The presence of adsorbed hydrogen atoms alters the hybridization of carbon atoms from  $sp^2$  to  $sp^3$ , partially removing the corresponding  $p_z$  orbital from the  $\pi$ -band. We model the yet finite probability of finding electrons at the adsorbant site by a finite value of the disorder strength  $\Delta$  (see Fig. 1).

Experimental results by Bostwick *et al.* [1] suggest a metal-to-insulator transition in graphene for a hydrogen coverage as low as  $0.3\%$ . In Fig. 2 we contrast the spatial distribution of the local density of states (LDOS)  $\rho_i(E) = \sum_n |\langle n|i \rangle|^2 \delta(E - E_n)$  at the Dirac point energy for a hydrogen coverage slightly below and above this threshold. For zigzag boundaries the well known edge states persist even in the presence of weak disorder. Impurities on the sublattice with high LDOS values near the GNR edges drastically reduce these values. On the other sublattice they do not have any effect. In the bulk of the ribbon, the LDOS is slightly enhanced as compared to the ordered case. Positive interference traps the wavefunction on sites in between the impurities. For periodic boundary conditions (PBC) the spatial LDOS distribution is clearly distinct for both impurity concentrations: We observe only slight local perturbations of the perfectly extended state for low impurity concentrations but a clearly localized state at  $1\%$  hydrogen coverage. Measurements on a sample of this size therefore yield

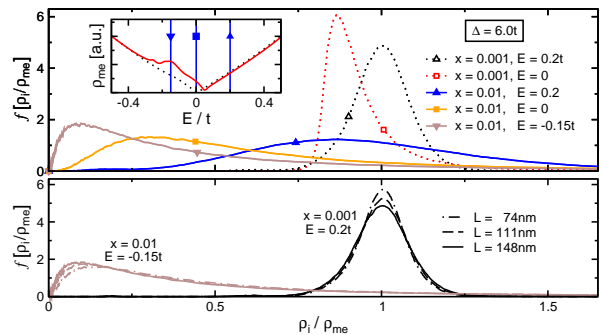


FIG. 3. (Color online) Upper panel: Distribution of the LDOS at experimentally relevant energies for the binary alloy model with different impurity concentrations and PBC. The sample width  $W = 109 \text{ nm}$ . Normalization of the distribution to  $\rho_{me}$  directly relates its position to the height of the maximum and its width. Inset: Magnification of the averaged DOS with indications of the energies for which the LDOS distributions are shown. Lower panel: Finite-size scaling of the LDOS distribution. Data obtained by the kernel polynomial method with resolution adapted to the level-spacing,  $N_k = 140$  (for details see [21, 22]).

metallic (insulating) behavior for coverages  $0.1\%$  ( $1\%$ ). The observed metallic character seems to be merely a consequence of a finite localization length  $\lambda$  that exceeds the system size. Note that the calculated state characteristics and experimental results agree qualitatively for PBC only. This underlines that the observed localization properties are intrinsic to short-range disordered bulk graphene. Edge effects arise on top, but are to a certain extent irrelevant in experiments, especially if mobilities are measured using a multiterminal Hall geometry [20].

In order to assert that AL takes place in infinite GNRs, we analyze the distribution of the normalized LDOS in Fig. 3. We restrict ourselves to three characteristic energies which are shown in the inset together with the averaged density of states  $\rho_{me} = \langle \rho_i \rangle$ . The behavior of the LDOS distribution upon finite-size scaling (lower panel) is a powerful criterion to detect AL for different kinds of disordered systems [22], even in presence of interactions [23]. Extended states are characterized by an  $f[\rho_i/\rho_{me}]$  being independent of the system size. Otherwise sensitivity of the distribution to the system size indicates localization, which we indeed observe for binary alloy disordered GNRs for all energies and both impurity concentrations.

For a given state, the shape of the LDOS distribution and the extent of its shifting depend on  $\lambda$ ; the more pronounced the shift and the more asymmetric  $f[\rho_i/\rho_{me}]$ , the shorter is  $\lambda$ . Larger impurity concentrations enhance localization, as can be seen from the asymmetric shape of  $f[\rho_i/\rho_{me}]$  for  $x = 0.01$ . The persisting size dependence for  $x = 0.001$  proves localization also for such a weak randomness. Here the high sensibility of the LDOS distribution to the ratio of  $\lambda$  and system size is of vital

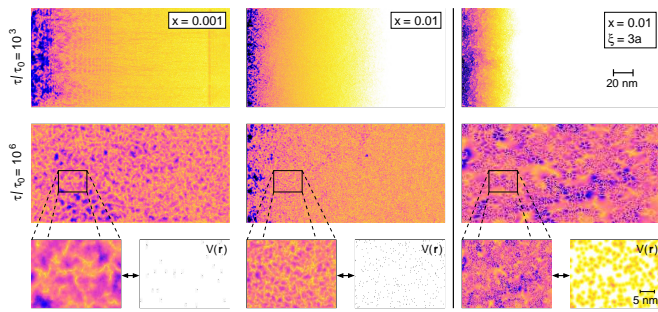


FIG. 4. (Color online) Time evolution of the local particle density on disordered zigzag GNRs after, at  $\tau = 0$ , finite (ordered) leads were attached to the left and right of the GNR.  $|\psi(\mathbf{r}_i, t)|^2$  is normalized to the actual mean particle density on the GNR. The color scale is identical to Fig. 2. Sample dimensions are  $(221 \times 109) \text{ nm}^2$ , corresponding to  $1800 \times 512$  lattice sites. Left and middle column: Binary alloy model with  $\Delta = 6t$ . Right column: Gaussian correlated disorder model with  $\xi = 3a$ , where  $a$  is the inter-carbon distance. Here the potential is normalized to  $\max(V_i) = 6t$ . The insets show magnifications of  $|\psi(\mathbf{r}_i, t)|^2$  in the quasistationary regime together with the corresponding potential landscape.

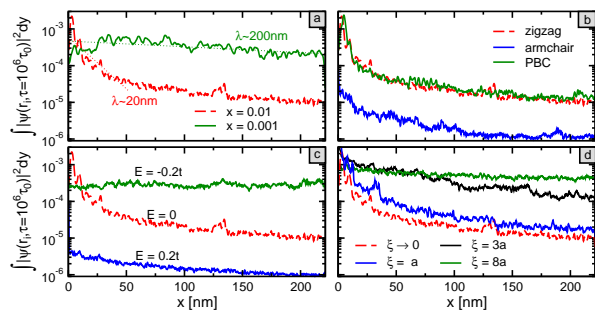


FIG. 5. (Color online) Quasistationary local particle density summed over the transverse direction. Each subpanel shows how changing one control parameter influences the baseline case (red dashed line: binary disorder,  $x = 0.01$ ,  $E = 0$ , zigzag BC) while keeping the others fixed.

importance. It allows to detect localization also in the case of weak disorder for which  $\lambda$  distinctly exceeds the system size and consequently  $f[\rho_i/\rho_{me}]$  is concentrated around unity.

In Fig. 4 we contrast the quantum dynamics of a particle injected into zigzag GNRs with binary or Gaussian correlated disorder and impurity concentrations of 0.1% and 1%. As initial state  $|\psi_0\rangle$  we prepare an exact  $E = 0$  eigenstate of the ordered infinite graphene lattice in the lead left to the sample (see Fig. 1). After bringing the lead in contact with the sample, we let the system evolve in time by solving the time-dependent Schrödinger equation by a Chebyshev expansion technique [19, 24]. Due to the coupling with the disordered GNR,  $|\psi_0\rangle$  is not an eigenstate of the overall system but comprises admixtures of other states, mainly from the vicinity of  $E = 0$ . The snapshot at  $\tau = 10^3\tau_0$ , where  $\tau_0 = \hbar/t$ , confirms the

intuition that spreading is faster the lower the impurity concentration is (see Fig. 4). At  $\tau = 10^6\tau_0$  all states have reached quasistationarity, and we can extract their characteristic features. For  $x = 0.1\%$  the state spans the whole sample. The inset reveals its puddle-like structure with density fluctuations of two orders of magnitude on length scales of 5 – 10 nm. At an impurity concentration of  $x = 1\%$  the particle density is reduced about two orders of magnitude between left and right edge of the GNR, providing a direct visualization of AL. Note that the local structure of  $|\psi\rangle$  remains puddle-like, but the spatial extent of the puddles is substantially reduced below 1 nm. From the similarity of both local structures one may argue that for larger systems also states for  $x = 0.1\%$  will be localized. Note that correlated disorder results in a markedly smoother potential landscape. In addition, the electron-hole puddles are superimposed by a coarse-grained filamentary structure.

Integrating the local particle density over the transverse ribbon direction allows for a more quantitative analysis of the localization properties (see Fig. 5). For a fixed configuration of impurity positions we vary the relevant control parameters and extract  $\lambda$  from fitting the quasistationary density to an exponential decay. Removing part of the impurities results in a larger  $\lambda$  [Fig. 5(a)]. For the considered ribbon width the difference between zigzag- and PBC is marginal, while armchair edges drastically reduce the transmission [Fig. 5(b)]. This reflects the mismatch of preferred transport direction and ribbon axis. Varying the incident particle energy [Fig. 5(c)] we observe an enhanced transmission for  $E = -0.2t$ , which might be attributed to resonant (localized) states. Note that at the position of the chemical potential of graphene on a SiC substrate,  $E = 0.2t$ ,  $\lambda$  is even shorter than at the Dirac point  $E = 0$ . For correlated long-range disorder [Fig. 5(d)],  $\lambda$  increases with  $\xi$ , yielding extended states if  $\xi \gg a$ . For  $\xi = a, 3a$  the states are still clearly localized. This disagrees with results in the literature obtained within the Dirac approximation [12], where the valley quantum number is conserved and localization is suppressed in absence of intervalley scattering [11]. We attribute this difference to the lattice discreteness and the breaking of the rotational symmetry of the Dirac cones by the trigonal symmetry of the honeycomb lattice. Moreover, even for a narrow banded initial state the dynamics is influenced by states from the whole energy spectrum where the graphene dispersion significantly deviates from the linear approximation. If all these aspects were taken into account, long-ranged disorder may cause localization within a tight-binding description in accordance with one-parameter scaling [25]. Whether AL really occurs for correlated disorder can be proven by performing a finite-size scaling of the LDOS distribution. In doing so we find evidence for localization for  $\xi = 3a$  from the shifting of the LDOS distribution (see left panel of Fig. 6). A remarkable feature of  $f[\rho_i/\rho_{me}]$  is the salient tail that



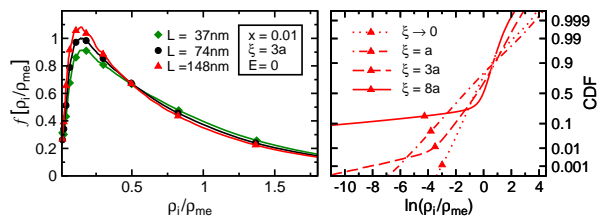


FIG. 6. (Color online) Left: Finite-size scaling of the LDOS distributions for the Gaussian correlated disorder model with parameters matching Fig. 4. Right: CDF of the LDOS for various potential ranges  $\xi$ .

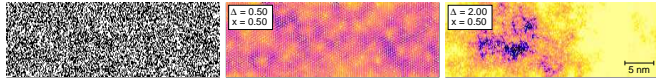


FIG. 7. (Color online) Spatial distribution of the normalized LDOS at  $E = 0$  for the disorder configuration shown in the left panel with PBC. System sizes and color mapping are the same as in Fig. 2. Data obtained by ED.

develops for small values of  $\rho_i$  on increasing  $\xi$ . In the right panel of Fig. 6 this results in a kinked cumulated distribution function (CDF) instead of the approximate straight CDF for uncorrelated disorder [26].

So far we considered strong disorder ( $\Delta \gg 1$ ) and weak randomness ( $x \ll 1$ ), for which it is tempting to relate average puddle size and distance between the impurities. Interestingly, electron-hole puddles also arise for weak disorder strength and strong randomness, corresponding to a disorder landscape varying on an atomistic scale without any correlations. Such a modeling might be regarded as an attempt to capture the effect of the buffer layer forming between epitaxially grown graphene and its SiC substrate [27]. In this setup we refrain from considering a correlated potential landscape in order not to impose any a priori correlations in the LDOS. For weak disorder strength,  $\Delta = 0.5t$ , the LDOS at  $E = 0$  nevertheless becomes puddle-like with a characteristic scale of 2-5 nm (see middle panel of Fig. 7). Note that the choice of BC has no qualitative impact on the LDOS in this limit of the binary alloy model. Obviously, any subtle differences in the state characteristics induced by BC are masked by the randomness of the potential landscape. Increasing the potential difference to  $\Delta = 2t$ ,  $\lambda$  drops below the system size and we observe clearly localized states.

To conclude, hydrogenated graphene behaves at zero temperature as a 'normal' two-dimensional disordered system concerning AL, provided the extensions of ultra-high-quality samples become very large. If the localization length noticeably exceeds the system size, the sample nevertheless shows metallic behavior. We find that also certain long-range correlations in the disorder landscape yield localized single-particle wavefunctions. Most notably, we show that disorder-induced electron-hole pud-

dles may arise for both disorder types. The intrinsic scale of the puddle-like structures in the eigenstates is not simply set by the distance between impurities, but results from subtle quantum interference effects. Even for atomic scale fluctuations of the disorder potential they might exceed 5 nm, which is in the range of experimentally measured values. The presence of electron-hole puddles, leading to intra- and inter-puddle transport, drives the system away from the metal-to-insulator transition, thereby masking AL [9]. This resolves the puzzle why AL is so hard to detect in disordered graphene and GNRs.

We acknowledge financial support by DFG through the graphene priority program SPP 1459, KONWIHR-II as well as granting of computing time on HLRB Munich.

- 
- [1] A. Bostwick *et al.*, Phys. Rev. Lett. **103**, 056404 (2009)
  - [2] D. C. Elias *et al.*, Science **323**, 610 (2009).
  - [3] Note that we focus exclusively on transport properties and do not address other interesting issues such as defect-induced magnetism or enhanced chemical activity (see, e.g., D. W. Boukhvalov and M. I. Katsnelson, J. Phys. Chem. C **113**, 14176 (2009); O. V. Yazyev, Rep. Prog. Phys **73**, 056501 (2010)).
  - [4] E. Abrahams *et al.*, Phys. Rev. Lett. **42**, 673 (1979)
  - [5] K. Nomura and A. H. MacDonald, Phys. Rev. Lett. **98**, 076602 (2007)
  - [6] A. H. Castro Neto *et al.*, Rev. Mod. Phys. **81**, 109 (2009)
  - [7] S. Adam *et al.*, Phys. Rev. Lett. **101**, 046404 (2008)
  - [8] S. Das Sarma *et al.*, Rev. Mod. Phys. **83**, 407 (2011)
  - [9] L. A. Ponomarenko *et al.*, DOI: 10.1038/NPHYS2114
  - [10] J. Katoch *et al.*, Phys. Rev. B **82**, 081417 (2010)
  - [11] H. Suzuura and T. Ando, Phys. Rev. Lett. **89**, 266603 (2002); J. Wurm *et al.* (2011) arXiv:1111.5969v1
  - [12] J. H. Bardarson *et al.*, Phys. Rev. Lett. **99**, 106801 (2007) K. Nomura, M. Koshino, and S. Ryu, *ibid.* **99**, 146806 (2007)
  - [13] K. Wakabayashi, Y. Takane, and M. Sigrist, Phys. Rev. Lett. **99**, 036601 (2007)
  - [14] S. Xiong and Y. Xiong, Phys. Rev. B. **76**, 214204 (2007); J. Bang and K. J. Chang, *ibid.* **81**, 193412 (2010); A. Chaves *et al.*, *ibid.* **82**, 205430 (2010);
  - [15] A. Deshpande *et al.*, Phys. Rev. B **79**, 205411 (2009) Y. Zhang *et al.*, Nature Phys. **5**, 722 (2009) J. Xue *et al.*, Nature Mat. **10**, 282 (2011)
  - [16] S. Das Sarma, E. H. Hwang, and Q. Li (2011), arXiv:1109.0988v1
  - [17] A. Rycerz, J. Tworzydło and C. W. J. Beenakker, EPL **79**, 57003 (2007).
  - [18] G. Schubert *et al.*, Phys. Rev. B **79**, 235116 (2009)
  - [19] G. Schubert and H. Fehske, Phys. Rev. B **77**, 245130 (2008)
  - [20] J. W. Klos *et al.*, Phys. Rev. B **80**, 245432 (2009)
  - [21] A. Weiße *et al.*, Rev. Mod. Phys. **78**, 275 (2006).
  - [22] G. Schubert *et al.*, Phys. Rev. B **81**, 155106 (2010)
  - [23] F. X. Bronold *et al.*, Philos. Mag. **84**, 673 (2004) D. Semmler *et al.*, Phys. Rev. B **84**, 115113 (2011)
  - [24] H. Fehske *et al.*, Phys. Lett. A **373**, 2182 (2009) Q. Liang

- et al.*, J. Phys. C **23**, 345502 (2011)
- [25] Y.-Y. Zhang *et al.*, Phys. Rev. Lett. **102**, 106401 (2009)
- [26] Note that there is numerical evidence against a *strict* log-normal LDOS distribution, i.e. the CDF should slightly deviate from straight line, see Rodriguez *et al.* (2009), arXiv:1107.5736v1.
- [27] K. V. Emtsev *et al.*, Nature Mat. **8**, 203 (2009)